

Triplet pairing of neutrons in β -stable neutron star matter

Ø. Elgarøy,^a L. Engvik,^a M. Hjorth-Jensen,^b E. Osnes^a

^a*Department of Physics, University of Oslo, N-0316 Oslo, Norway*

^b*ECT*, European Centre for Theoretical Studies in Nuclear Physics and Related Areas, Strada delle Tabarelle 286, I-38050 Villazzano (Trento), Italy*

Abstract

3P_2 pairing in neutron matter is investigated using the Bonn potential models. We find pairing energy gaps in pure neutron matter comparable to the results of previous investigators when the attractive tensor coupling is included. However, taking into account that in a neutron star we have matter at β equilibrium, we find that the 3P_2 - 3F_2 energy gap is reduced considerably.

1 Introduction

Superfluidity in neutron stars is expected to have a profound influence on their dynamical and thermal properties [1]. Due to the properties of nuclear forces several nucleon superfluids can be formed, the most commonly considered being the 1S_0 neutron and proton superfluids, and the 3P_2 neutron superfluid. In a recent investigation [2] we calculated 1S_0 neutron and proton pairing gaps, ignoring complicated many-body effects. In this paper we follow the same philosophy in calculating energy gaps for neutrons in the 3P_2 state, using realistic nucleon-nucleon (NN) forces derived from meson theory [3].

2 Theory

The standard BCS theory [4,5] has to be extended when dealing with pairing of particles in states with non-zero angular momentum. The method of generalizing the Bogolyubov transformation to pairing of particles with arbitrary angular momentum and isospin is described in refs. [6,7]. We are in this paper concerned with neutron pairing in the 3P_2 - 3F_2 state, and thus take $J = 2$,

$S = 1$, $L = 1, 3$, and $T = 1$. In this case, the 1S_0 gap equation is replaced by a set of ten ($2 \times (2J + 1)$) coupled equations for the ten energy gap components:

$$\begin{aligned} \Delta_{\lambda L m_J}(k) = & -\frac{1}{\pi}(-1)^{1-S} \int_0^\infty dk' k'^2 \sum_{L'} i^{L'-L} \langle k' | V_\lambda^{L'L} | k \rangle \\ & \times \int d\hat{\mathbf{k}}' \sum_{L'' m'_J} \Delta_{\lambda L'' m'_J}(k') \text{Tr}[\mathbf{G}_{\lambda L' m_J}^*(\hat{\mathbf{k}}') \mathbf{G}_{\lambda L'' m'_J}(\hat{\mathbf{k}}')] \\ & \times \frac{1}{\sqrt{(\epsilon_{k'} - \epsilon_{k_F})^2 + D_\lambda^2(\mathbf{k}')}} \end{aligned} \quad (1)$$

where $\lambda \equiv (T = 1, S = 1, J = 2)$, the orbital angular momenta L , L' , and L'' take on the values 1 and 3, and

$$\mathbf{G}_{\lambda L m_J}(\hat{\mathbf{k}}) \equiv \left\{ \left\langle \frac{1}{2} \sigma_1 \frac{1}{2} \sigma_2 | S m_S \right\rangle \langle S m_S L m_L | J m_J \rangle Y_{L m_J - m_S}(\hat{\mathbf{k}}) \right\}$$

is a 2×2 matrix in spin- $\frac{1}{2}$ space. Furthermore, $Y_{L m_J - m_S}$ is a spherical harmonic, D_λ is given by

$$D_\lambda^2(\mathbf{k}) = \frac{1}{2} \sum_{LL'} \sum_{m_J m'_J} \Delta_{\lambda L m_J}^*(k) \Delta_{\lambda L m'_J}(k) \text{Tr}[\mathbf{G}_{\lambda L m_J}^\dagger(\hat{\mathbf{k}}) \mathbf{G}_{\lambda L' m'_J}(\hat{\mathbf{k}})],$$

and ϵ_k and ϵ_{k_F} are single-particles, evaluated at $k = k$ and $k = k_F$, respectively. The symbol Tr denotes the trace operation, the symbol † denotes Hermitian conjugation, and $\langle k' | V_\lambda^{L'L} | k \rangle$ are matrix elements of the NN interaction in momentum space, in the partial wave characterized by L , L' and λ .

2.1 Uncoupled equations for 3P_2 pairing

The set of equations (1) is rarely solved in its full generality, and we will in this paper look at two approximations. In the first one, considered by e.g. Baldo *et al.* [8], the tensor interaction is neglected, and thus pairing in a pure 3P_2 wave is considered. Furthermore, only the solutions with $m_J = 0$ or $|m_J| = 2$ are considered, because these have been found to be close to the most general solution of eq. (1) [7]. It can then be shown that the gap equations reduce to

$$\Delta_i(k) = -\frac{1}{\pi} \int_0^\infty dk' k'^2 \langle k' | V(^3P_2) | k \rangle \frac{\Delta_i(k')}{\tilde{E}_i(k')}, \quad i = 0, 2, \quad (2)$$

where $i = 0, 2$ for $m_J = 0$, $|m_J| = 2$ respectively. We have here defined

$$\frac{1}{\overline{E_i(k)}} \equiv \begin{cases} \frac{3}{4} \int_{-1}^{+1} d(\cos \theta) \frac{1 - \cos^2 \theta}{E_2(\mathbf{k})}, & i = 2, \\ \frac{1}{4} \int_{-1}^{+1} d(\cos \theta) \frac{1 + 3 \cos^2 \theta}{E_0(\mathbf{k})}, & i = 0, \end{cases} \quad (3)$$

where $E(\mathbf{k})$ is the quasiparticle energy, given by

$$E_i(\mathbf{k}) = \begin{cases} \sqrt{(\epsilon_k - \epsilon_{k_F})^2 + \frac{3}{8\pi} \Delta_2^2(1 - \cos^2 \theta)}, & i = 2, \\ \sqrt{(\epsilon_k - \epsilon_{k_F})^2 + \frac{1}{16\pi} \Delta_0^2(k)(1 + 3 \cos^2 \theta)}, & i = 0. \end{cases} \quad (4)$$

In eq. (2) $\langle k' | V(^3P_2) | k \rangle$ are the momentum-space matrix elements of the bare NN interaction in the 3P_2 wave. Eq. (2) must in each case be solved self-consistently for the gap component $\Delta_0(k)$ or $\Delta_2(k)$. The energy gap is by convention defined to be the second term appearing under the square root in the expression for the quasiparticle energy:

$$D_0^2(\mathbf{k}) = \frac{1}{16\pi} \Delta_0^2(k)(1 + 3 \cos^2 \theta) \quad (5)$$

$$D_2^2(\mathbf{k}) = \frac{3}{8\pi} \Delta_2^2(k)(1 - \cos^2 \theta) \quad (6)$$

When giving numerical results, we use angle-averaged energy gaps, given by

$$\overline{D_2^2(k)} = \frac{1}{4\pi} \Delta_2^2(k)$$

$$\overline{D_0^2(k)} = \frac{1}{8\pi} \Delta_0^2(k).$$

Replacing angle-dependent quantities in the gap equation with their angular average has been found to be a good approximation [8]. However, the angle dependence is easily handled numerically, so we have throughout solved the gap equation with angle dependencies included.

2.2 Coupled equations for 3P_2 - 3F_2 pairing

In the second approximation we include the tensor coupling effect, but look at the solution with $m_J = 0$ only, thus reducing the number of components from ten to two. This solution is expected to be a good approximation to the most general solution of eq. (1) [7]. For $m_J = 0$, the two coupled equations for the $L = 1$ and $L = 3$ gap components become

$$\begin{aligned}\Delta_{\lambda 10}(k) = & -\frac{1}{\pi} \int_0^\infty dk' k'^2 \langle k' | V_\lambda^{11} | k \rangle \int d\hat{\mathbf{k}}' \frac{\{\Delta_{\lambda 10}(k')f(\theta) + \Delta_{\lambda 30}(k')g(\theta)\}}{E(\mathbf{k}')} \\ & + \frac{1}{\pi} \int_0^\infty dk' k'^2 \langle k' | V_\lambda^{31} | k \rangle \int d\hat{\mathbf{k}}' \frac{\{\Delta_{\lambda 10}(k')g(\theta) + \Delta_{\lambda 30}(k')h(\theta)\}}{E(\mathbf{k}')} \quad (7)\end{aligned}$$

$$\begin{aligned}\Delta_{\lambda 30}(k) = & \frac{1}{\pi} \int_0^\infty dk' k'^2 \langle k' | V_\lambda^{13} | k \rangle \int d\hat{\mathbf{k}}' \frac{\{\Delta_{\lambda 10}(k')f(\theta) + \Delta_{\lambda 30}(k')g(\theta)\}}{E(\mathbf{k}')} \\ & - \frac{1}{\pi} \int_0^\infty dk' k'^2 \langle k' | V_\lambda^{33} | k \rangle \int d\hat{\mathbf{k}}' \frac{\{\Delta_{\lambda 10}(k')g(\theta) + \Delta_{\lambda 30}(k')h(\theta)\}}{E(\mathbf{k}')} \quad (8)\end{aligned}$$

The functions of the polar angle θ of \mathbf{k}' are defined by

$$\begin{aligned}f(\theta) &= \frac{1}{8\pi} (1 + 3 \cos^2 \theta), \\ g(\theta) &= -\frac{\sqrt{6}}{64\pi} (1 - 7 \cos^2 \theta + 5 \sin \theta \sin 3\theta - 10 \cos \theta \cos 3\theta) \\ h(\theta) &= \frac{3}{128\pi} (13 + 4 \cos^2 \theta + 5 \sin \theta \sin 3\theta + 15 \cos \theta \cos 3\theta),\end{aligned}$$

the quasiparticle energy $E(\mathbf{k})$ is given by

$$E(\mathbf{k}) = \sqrt{(\epsilon_k - \epsilon_{k_F})^2 + D_\lambda^2(\mathbf{k})}, \quad (9)$$

and the energy gap by

$$D_\lambda^2(\mathbf{k}) = \frac{1}{2} f(\theta) \Delta_{\lambda 10}^2(k) + \frac{1}{2} h(\theta) \Delta_{\lambda 30}^2(k) + g(\theta) \Delta_{\lambda 10}(k) \Delta_{\lambda 30}(k). \quad (10)$$

In ref. [8] Baldo *et al.* obtained a large 3P_2 energy gap without the tensor coupling. However, in refs. [7,9] the added attraction from the tensor coupling effect was found to be essential to the existence of superfluidity in this state. The importance of the tensor coupling depends to some extent on the choice of NN interaction, and we will therefore consider both cases.

2.3 Calculation of single-particle energies

The single-particle energies appearing in the quasiparticle energies (4) and (9) are obtained through a self-consistent BHF calculation, using a G -matrix

defined through the Bethe-Brueckner-Goldstone equation as

$$G = V + V \frac{Q}{\omega - H_0} G, \quad (11)$$

where V is the nucleon-nucleon potential, Q is the Pauli operator which prevents scattering into intermediate states prohibited by the Pauli principle, H_0 is the unperturbed Hamiltonian acting on the intermediate states and ω is the so-called starting energy, the unperturbed energy of the interacting particles. Methods to solve this equation are reviewed in ref. [10]. The single-particle energy for state k_i (i encompasses all relevant quantum numbers like momentum, isospin projection, spin etc.) in nuclear matter is assumed to have the simple quadratic form¹

$$\epsilon_{k_i} = \frac{k_i^2}{2m^*} + \delta_i, \quad (12)$$

where m^* is the effective mass. The terms m^* and δ , the latter being an effective single-particle potential related to the G -matrix, are obtained through the self-consistent BHF procedure. The so-called model-space BHF method for the single-particle spectrum has been used, see e.g. ref. [10], with a cutoff momentum $k_M = 3.0 \text{ fm}^{-1} > k_F$. In this approach the single-particle spectrum is defined by

$$\epsilon_{k_i} = \frac{k_i^2}{2m} + u_i, \quad (13)$$

where m is the nucleon mass, and the single-particle potential u_i is given by

$$u_i = \begin{cases} \sum_{k_h \leq k_F} \langle k_i k_h | G(\omega = \epsilon_{k_i} + \epsilon_{k_h}) | k_i k_h \rangle, & k_i \leq k_M, \\ 0, & k_i > k_M, \end{cases}, \quad (14)$$

where the subscript AS denotes antisymmetrized matrix elements. This prescription reduces the discontinuity in the single-particle spectrum as compared with the standard BHF choice $k_M = k_F$. The self-consistency scheme consists in choosing adequate initial values of the effective mass and δ . The obtained G -matrix is then used to calculate the single-particle potential u_i , from which we obtain new values for m^* and δ . This procedure continues until these parameters vary little. We stress that in the energy gap calculations we have used the single-particle spectrum defined by eqs. (13) and (14), and not the effective mass approximation (12).

¹ Throughout this work we set $\hbar = c = 1$.

The BHF equations can be solved for different proton fractions, using the formalism of refs. [10,11]. The conditions for β equilibrium require that

$$\mu_n = \mu_p + \mu_e, \quad (15)$$

where μ_i is the chemical potential of particle type i , and that charge is conserved

$$n_p = n_e, \quad (16)$$

where n_i is the particle number density for particle i . If muons are present, the condition for charge conservation becomes

$$n_p = n_e + n_\mu, \quad (17)$$

and conservation of energy requires that

$$\mu_e = \mu_\mu. \quad (18)$$

We assume that neutrinos escape freely from the neutron star. The proton and neutron chemical potentials are determined from the energy per baryon, calculated self-consistently in the MBHF approach. The electron chemical potential, and thereby the muon chemical potential, is then given by $\mu_e = \mu_n - \mu_p$. The Fermi momentum of lepton type $l = e, \mu$ is found from

$$k_{F_l} = \sqrt{\mu_l^2 - m_l^2} \quad (19)$$

where m_l is the mass of lepton l , and we get the particle density using $n_l = k_l^3/3\pi^2$. The proton fraction is then determined by the charge neutrality condition (17).

Throughout this work, we use the meson-exchange potential models of the Bonn group, versions A, B and C in Table A.1 of ref. [3]. These potentials have given satisfactory results in applications to finite nuclei and nuclear matter [10]. Furthermore, the only parameters entering in the Bonn models are physically motivated ones, e.g. meson masses. A point of interest in this work is that the Bonn potentials have a rather weak tensor component. The A.1 parameters are the consistent choice of parameters in a non-relativistic approach, as they were fitted using the Blankenbecler-Sugar reduction [12] of the four-dimensional Bethe-Salpeter equation, yielding a T -matrix equation of the same form as the non-relativistic Lippmann-Schwinger equation [3].

3 Pairing in the pure 3P_2 wave

We have solved the gap equations (2) in pure neutron matter. The calculational procedure consists of two steps: First we obtain self-consistent single-particle energies in the MBHF approach, as described in section 2.3. The next step is to solve the relevant gap equation, for $m_J = 0$ or $|m_J| = 2$, with the bare NN interaction as pairing interaction. Being non-linear integral equations, the gap equations must be solved by iteration. In ref. [2] we applied a model-space approach to the gap equation for 1S_0 pairing. One of the advantages of this approach was that the numerical treatment became easier, as it allowed us to treat pairing correlations and the effects of the repulsive core of the NN interaction separately. The same method can easily be applied to the gap equations studied in this paper. However, as seen from fig. 1, the interaction in the 3P_2 wave is weak at the densities of interest, so a model space treatment is not called for. Nevertheless, we would like to point out some problems encountered in the numerical solution. First, the 3P_2 energy gap is considerably

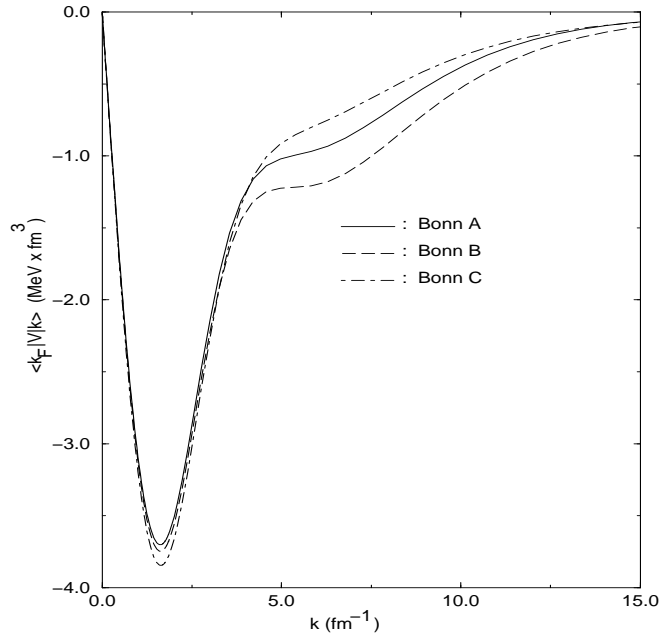


Fig. 1. Matrix elements $\langle k_F | V(^3P_2) | k \rangle$ of the Bonn A, B and C potentials, shown as functions of the relative momentum k for $k_F = 1.8 \text{ fm}^{-1}$.

smaller than the 1S_0 energy gap, which is of order 1 MeV [2]. A small energy gap at the Fermi surface causes problems in the numerical treatment, as we see from eq. (2) that for small values of $\Delta_i(k_F)$ the integrand

$$f(k, k')_i \equiv -\frac{1}{\pi} k'^2 \langle k | V(^3P_2) | k' \rangle \frac{\Delta_i(k')}{\tilde{E}_i(k')} \quad i = 0, 2$$

in the gap equation has a very narrow peak at $k = k_F$, as shown in fig. 2. Thus, to obtain stable results, we had to take great care in choosing mesh

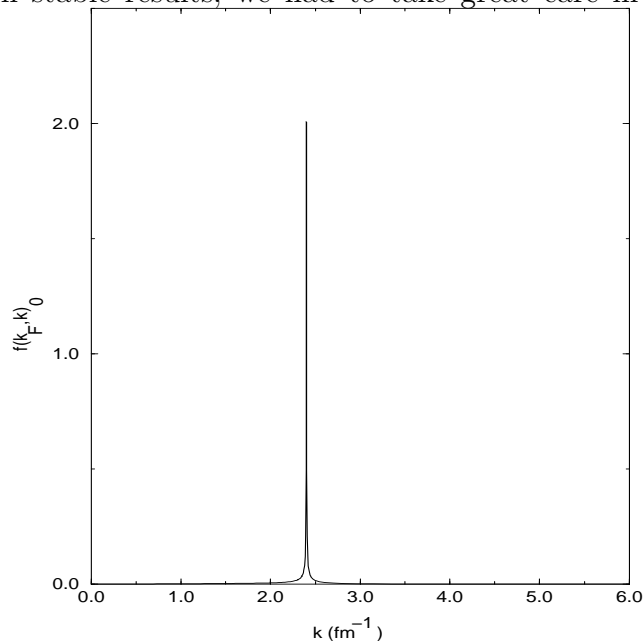


Fig. 2. Integrand $f(k, k')_0$ in the gap equation for $m_J = 0$ and $k = k_F = 2.4 \text{ fm}^{-1}$.

points for the momentum space integration near k_F . As seen from fig. 2 the choice of upper cutoff momentum was almost immaterial, and $k = 15 \text{ fm}^{-1}$ was found to be adequate. We should mention that Khodel, Khodel and Clark [13] recently published a new method for solving gap equations which eliminates the problems occurring when the gap parameter is small.

In fig. 3 the energy gap $\overline{D}_0(k_F)$, calculated with MBHF single-particle energies, is shown. The energy gap $\overline{D}_2(k_F)$ was found to be similar to $\overline{D}_0(k_F)$, as seen from fig. 4. Takatsuka and Tamagaki [7] and Amundsen and Østgaard [9] found that the 3P_2 gap vanished for realistic values of the neutron effective mass (in the range 0.90-0.65, see table 1), and thus it was necessary to include the attractive tensor coupling to the 3F_2 wave. As will be shown in the next section, our results for the pure 3P_2 wave are of the same size as the results where the tensor coupling is included. This result is probably due to the Bonn potentials having a weaker tensor force than the potentials used in refs. [7,9]. However, our results are one order of magnitude smaller than the results of Baldo *et al.* [8], who found energy gaps of the order 1 MeV without the tensor coupling effect.

The energy gap function D_0 given by eq. (5) is nodeless (as a function of θ), while D_2 has nodes for $\cos^2 \theta = 1$. A nodeless energy gap results in the usual exponential decay of the specific heat below the superfluid transition temperature. If there are nodes, the specific heat will follow a power-law [14]. Thus the solution with $m_J = 0$, if realized, gives a different thermal behaviour than the solution with $|m_J| = 2$. The favoured solution is the one which gives

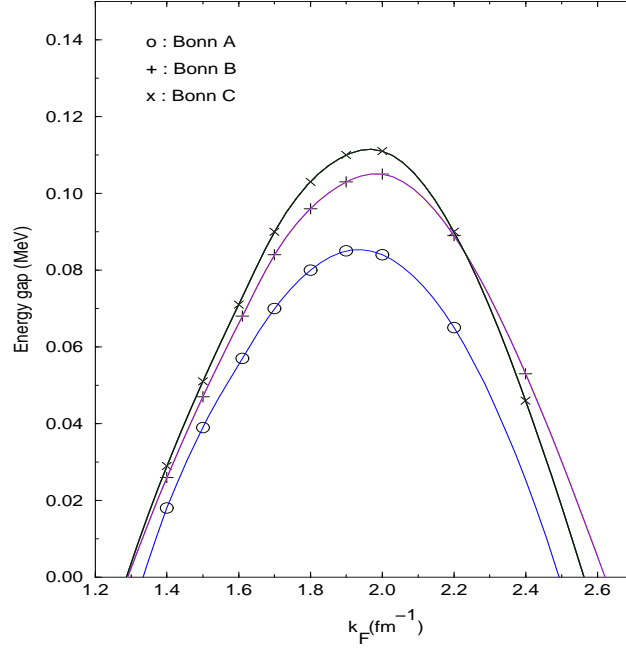


Fig. 3. Angle-averaged energy gap $\overline{D}_0(k_F)$ calculated with Bonn A, B and C.

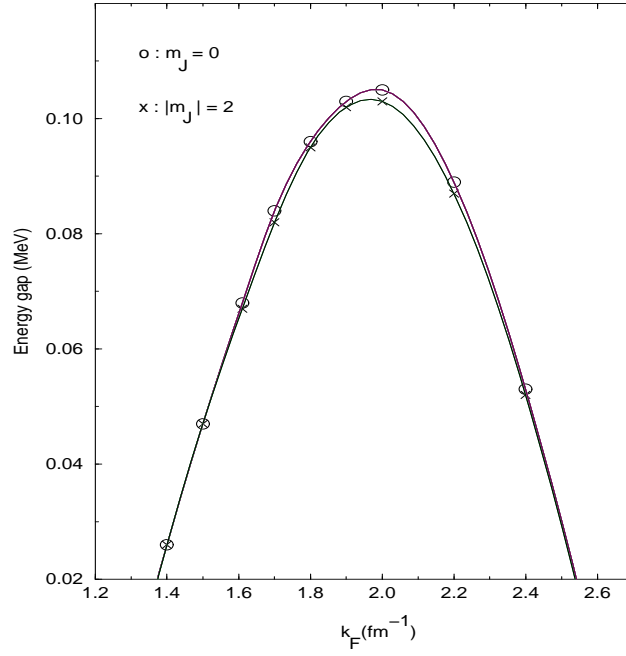


Fig. 4. Comparison of the angle averaged energy gap for $m_J = 0$ with corresponding results for $|m_J| = 2$. The results are for the Bonn B potential.

the lowest condensation energy. This quantity is, in the so-called weak-coupling limit, given by

$$\Delta E \approx -\frac{\rho_0}{2} \overline{D}_\lambda^2(k_F), \quad (20)$$

where ρ_0 is the density of states at the Fermi energy. In table 1 the two solutions are compared with respect to the condensation energy. The results

| k_F (fm $^{-1}$) | $-\Delta E/(\rho_0/8\pi)(m_J = 0)$ (MeV) | $-\Delta E/(\rho_0/8\pi)(m_J = 2)$ (MeV) |
|---------------------|--|--|
| 1.40 | 0.008 | 0.008 |
| 1.60 | 0.058 | 0.056 |
| 1.80 | 0.113 | 0.116 |
| 2.00 | 0.139 | 0.133 |
| 2.20 | 0.100 | 0.095 |

Table 1

Condensation energies calculated with the Bonn B potential.

shown are for the Bonn B potential. It is seen that the two solutions are very nearly degenerate, a result which is in agreement with the more complete discussions found in refs. [7,9], with the nodeless solution, $m_J = 0$, seemingly the favoured one.

4 Inclusion of the tensor coupling

We have solved the coupled equations (7) and (8) for pure neutron matter. We give results for the angle average of D_λ ,

$$\overline{D}_{\lambda m_J=0}(k_F) = \frac{1}{\sqrt{8\pi}} \sqrt{\Delta_{\lambda 10}^2(k_F) + \Delta_{\lambda 30}^2(k_F)} \approx \frac{\Delta_{\lambda 10}}{\sqrt{8\pi}}, \quad (21)$$

where the last approximation is valid because $\Delta_{\lambda 30}(k_F)$ was found to be negligible in comparison with $\Delta_{\lambda 10}(k_F)$. The following procedure was used to solve the coupled gap equations: First we obtained single-particle energies in the MBHF approach, as described in section 2.3. Starting with suitable approximations for the gap components $\Delta_{\lambda 10}$ and $\Delta_{\lambda 30}$ (for $\Delta_{\lambda 10}$ we could start with the solution of the uncoupled equation considered in section 3), the gap equations (7) and (8) were solved by iteration. Again, special attention had to be paid to the integration over momenta near k_F , because of the almost singular behaviour of the integrand there. Stable results were obtained with the same choice of mesh points as for the uncoupled case considered in the previous section.

In fig. 5 the energy gaps in pure neutron matter obtained with Bonn A, B and C are shown. From these results it is seen that the tensor force increases the energy gaps. However, this effect is not so important here as in the works of Takatsuka and Tamagaki [7] and Amundsen and Østgaard [9]. This was to be expected, since the Bonn potentials have weaker tensor components than the OPEG potentials used in refs. [7,9]. The effects of the tensor coupling are greater for Bonn C than for Bonn B and A, reflecting the differing tensor

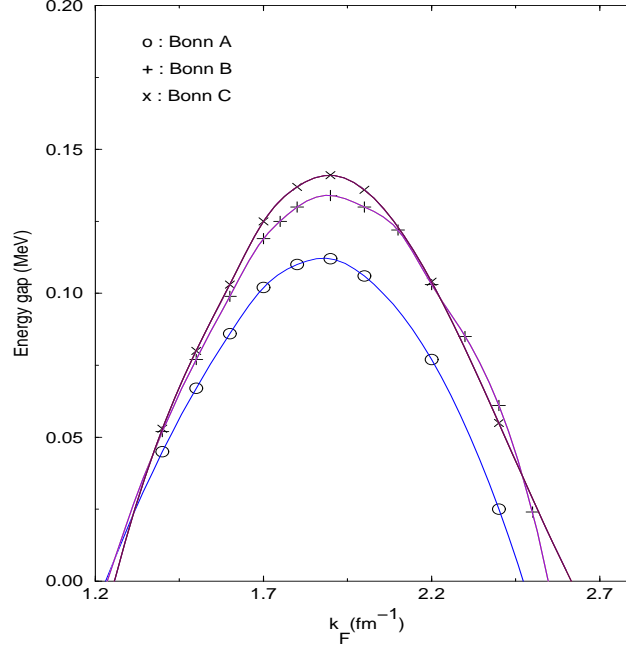


Fig. 5. 3P_2 - 3F_2 energy gaps in pure neutron matter.

strengths of the Bonn interactions. In fig. 6 the effective masses are plotted as functions of the neutron Fermi momentum. This figure shows that the Bonn models give nearly identical effective masses in pure neutron matter. The differences in the energy gaps are therefore mainly due to differences in the 3P_2 - 3F_2 wave of the interactions. From fig. 1 it is seen that Bonn C gives more attraction near k_F than do Bonn B and A. Since the main contribution to the integral in the gap equation comes from the region near k_F , it is reasonable that Bonn C gives the largest energy gaps.

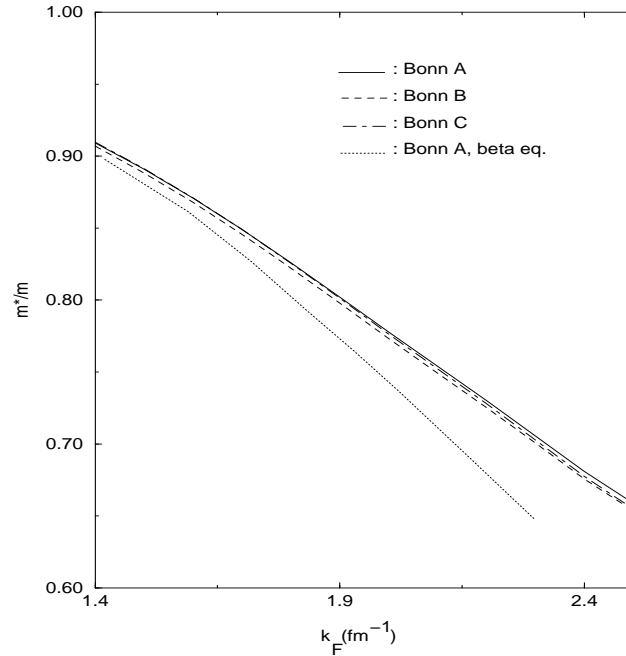


Fig. 6. Effective masses in pure neutron matter and in matter at β equilibrium.

We have also calculated the 3P_2 - 3F_2 neutron energy gap in neutron star matter at β equilibrium. The neutron fractions, shown in figure 7, were determined from a self-consistent MBHF calculation, imposing the relevant equilibrium constraints as described in section 2.3. The results, obtained with the Bonn A potential, are shown in figure 8. The size of the energy gap is reduced

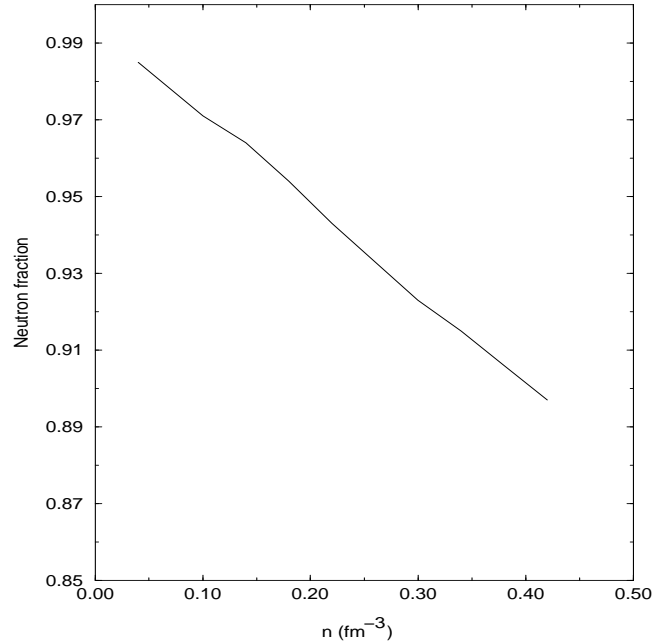


Fig. 7. Neutron fraction as a function of the nucleon density n at β equilibrium with muons included.

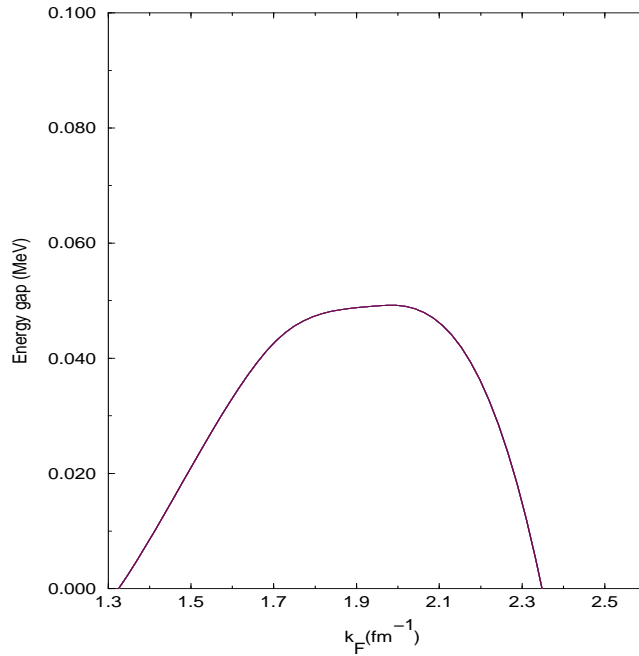


Fig. 8. Neutron energy gap at β equilibrium.

considerably, and the density range for this superfluid shrinks in comparison with the case of pure neutron matter. The main reason for this is probably

the reduced neutron effective masses in β -stable matter, as seen in fig. 6.

5 Discussion

The results of this paper are summarized in fig. 9, where we show the following results:

- the 3P_2 - 3F_2 energy gap in pure neutron matter
- neutron 3P_2 - 3F_2 energy gap at β equilibrium
- proton 1S_0 energy gap at β equilibrium, taken from ref. [2],

all as functions of the nucleon density. From the figure it is seen that the proton energy gap is one order of magnitude larger than the neutron energy gaps. Thus the dominating contribution to the suppression of the modified URCA processes will be due to superconducting protons [15]. Taking into account that in a neutron star we have matter at β equilibrium and not pure neutron matter, the neutron energy gap is reduced by approximately a factor of two.

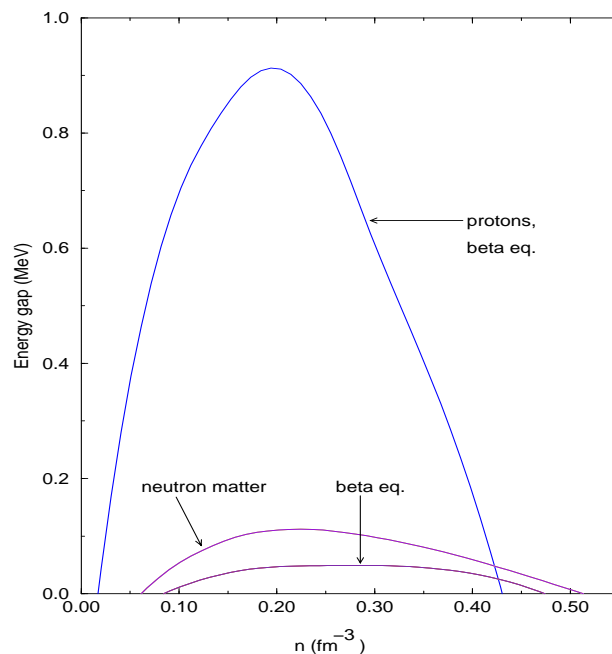


Fig. 9. Energy gaps for protons and neutrons in the quantum fluid region of a neutron star.

The results obtained in this work for the 3P_2 - 3F_2 energy gaps in pure neutron matter are in good agreement with those of Takatsuka and Tamagaki [7] and Amundsen and Østgaard [9]. We find a maximum energy gap of the same size as in refs. [7,9], and a density region for pairing intermediate between those

| Authors | Max. energy gap (MeV) | Density range (fm ⁻³) | m^*/m (typical values) | Potential |
|-----------|-----------------------|-----------------------------------|--------------------------|------------------|
| AØ | 0.12 | 1.4-3.0 | 0.70-0.89 | OPEG |
| BCLL | 1.5 | 1.8-3.2 | 0.70-0.86 | Argonne V_{14} |
| TT | 0.12 | 1.5-2.4 | 0.70-0.82 | OPEG |
| HGRR | 0.9 | 1.0-3.0 | 1.0 | Tabakin |
| This work | 0.13 | 1.2-2.5 | 0.65-0.91 | Bonn B |

Table 2

Results for the 3P_2 energy gap in neutron matter.

found in the two references above. In table 2 and fig. 10 we summarize the results of refs. [7](TT), [8](BCLL), [9](AØ), [16](HGRR), and the present work.

We should at this point emphasize that the effective masses quoted in the

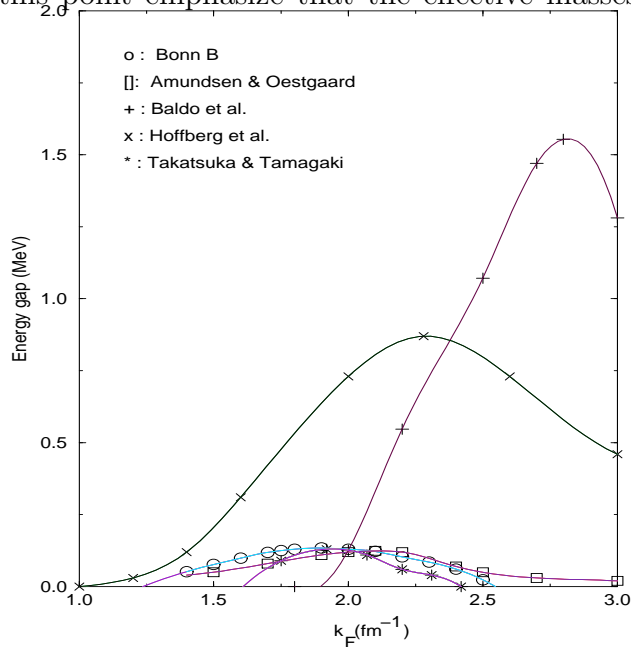


Fig. 10. Results for the triplet energy gap in neutron matter. The results of Baldo *et al.* and Hoffberg *et al.* were obtained without the tensor coupling.

table are meant to facilitate comparison between the different works. Both in this work and in refs. [7,8], the gap equations were solved with k -dependent single-particle potentials, without resorting to the effective mass approximation. From table 2 it is seen that the the energy gap has generally been found to be of order 0.1 MeV. The results of Baldo *et al.* [8] are remarkable, considering that they have neglected the attractive contributions from the tensor coupling to 3F_2 . With effective masses in the range used by Baldo *et al.*, the energy gap in the pure 3P_2 wave was in this work found to be one order of magnitude smaller, and in refs. [7,9] it was found to vanish. In addition, we found the 3P_2 gap to exist at lower densities than Baldo *et al.* Although both Amundsen and Østgaard and Takatsuka and Tamagaki used the OPEG potentials, Amundsen and Østgaard found that the energy gap extended up to

$k_F = 3.0 \text{ fm}^{-1}$. This difference can be understood because different approaches to the single-particle energies were employed. Amundsen and Østgaard took m^*/m to be constant (equal to 0.70) above $k_F = 2.4 \text{ fm}^{-1}$ [18], while Takatsuka and Tamagaki used a density-dependent effective mass all the way, and thus it dropped to values below 0.70 beyond $k_F = 2.4 \text{ fm}^{-1}$. Thus it is seen that the single-particle spectrum is a crucial ingredient in energy gap calculations. However, the Brueckner-Hartree-Fock spectrum, and variations thereof, used in most works, including the present, may be of questionable validity at the densities where the 3P_2 energy gap closes, where relativistic effects and many-body correlations become increasingly important. To further illustrate the importance of the single-particle energies, we have calculated the energy gap at $k_F = 1.8 \text{ fm}^{-1}$ as a function of the effective mass parameter m^*/m . The results in fig. 11 show that the energy gap depends strongly on the effective mass. Also included in table 2 are the results of Hoffberg *et al.* [16]. They are,

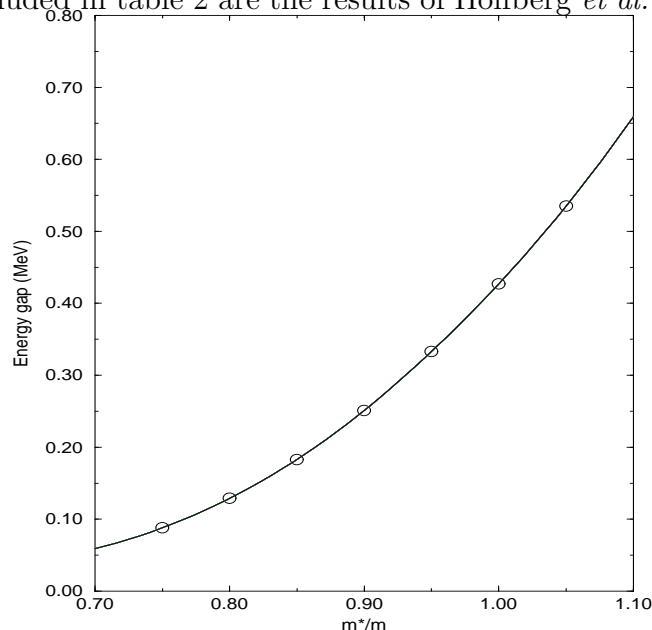


Fig. 11. Effective mass dependency of the 3P_2 - 3F_2 energy gap. The results were obtained using the Bonn C potential and $k_F = 1.8 \text{ fm}^{-1}$.

however, not directly comparable with the other results, as they have been obtained directly from the 3P_2 phase shifts, and with $m^*/m = 1$. However, it is interesting to note that they obtained a smaller maximum energy gap than Baldo *et al.*

To the best of our knowledge, the 3P_2 - 3F_2 energy gap has not been calculated in β -stable neutron star matter before. Our results show that the energy gap is reduced by a factor of two when β equilibrium is taken into account, mainly because the neutron effective mass is reduced. A point of interest here is that in a recent investigation of neutron star cooling, Schaab *et al.* [19] found that agreement with observations was obtained if the 3P_2 energy gaps were lowered by a factor of two (they used the results of ref. [9] for pure neutron

matter). A recent analysis by Page [20] of data for the Geminga pulsar showed that baryon pairing in most of the star was necessary to obtain agreement with the observed surface temperature, assuming that fast cooling processes were possible. However, with equations of state for β -stable matter, calculated within the non-relativistic BHF approach, we find that the critical density for the onset of the direct URCA processes to be 0.62 fm^{-3} , while within the relativistic Dirac-Brueckner-Hartree-Fock approach, the corresponding density was found to be 0.50 fm^{-3} [15]. At these densities the neutron and proton pairing gaps have already vanished, so the direct URCA processes will not be suppressed by superfluidity within this picture. Further investigation of 3P_2 pairing is therefore of interest. However, an important shortcoming of all calculations, including those reported in this work, is the neglect of many-body effects in the pairing interaction. The so-called polarization term has been found to reduce the 1S_0 proton and neutron energy gaps by as much as a factor of 2-3 [21]. It is, however, expected that polarization effects will tend to increase the 3P_2 neutron energy gap [22]. Further investigation of superfluidity in dense matter is therefore of interest.

6 Conclusion

In this work we have calculated pairing gaps for neutrons in the 3P_2 state in neutron matter and in matter at β equilibrium. For pure neutron matter, we found a non-zero energy gap for $1.2 \text{ fm}^{-1} \leq k_F \leq 2.5 \text{ fm}^{-1}$, with a maximum value of $0.12\text{--}0.13 \text{ MeV}$. Taking the conditions for β equilibrium into account, the corresponding values became $1.32 \text{ fm}^{-1} \leq k_F \leq 2.34 \text{ fm}^{-1}$ and 0.05 MeV . However, evaluation of the contribution from medium polarization effects to the pairing interaction is necessary before any definite conclusions can be drawn.

This work has been supported by the Research Council of Norway (NFR) under the Programme for Supercomputing through a grant of computing time. MHJ thanks the NFR and the Istituto Trentino di Cultura, Italy, for financial support.

References

- [1] S. L. Shapiro and S. A. Teukolsky, *Black Holes, White Dwarfs, and Neutron Stars, The Physics of Compact Objects* (Wiley, New York, 1983)
- [2] Ø. Elgarøy, L. Engvik, M. Hjorth-Jensen and E. Osnes, *Nucl. Phys. A*, in press
- [3] R. Machleidt, *Adv. Nucl. Phys.* 19 (1989) 189.

- [4] J. Bardeen, L. N. Cooper and J. R. Schrieffer, Phys. Rev. 108 (1957) 1175.
- [5] L. N. Cooper, R. L. Mills and A. M. Sessler, Phys. Rev. 114 (1959) 1377.
- [6] R. Tamagaki, Progr. Theor. Phys. 44 (1970) 905.
- [7] T. Takatsuka and R. Tamagaki, Progr. Theor. Phys. Suppl. 112 (1993) 27.
- [8] M. Baldo, J. Cugnon, A. Lejeune and U. Lombardo, Nucl. Phys. A 536 (1992) 349.
- [9] L. Amundsen and E. Østgaard, Nucl. Phys. A 437 (1985) 487.
- [10] M. Hjorth-Jensen, T. T. S. Kuo and E. Osnes, Phys. Rep. 261 (1995) 125.
- [11] H. Q. Song, Z. X. Wang and T. T. S. Kuo, Phys. Rev. C 46 (1992) 1788.
- [12] R. Blankenbecler and R. Sugar, Phys. Rev. 142 (1966) 1051.
- [13] V. A. Khodel, V. V. Khodel and J. W. Clark, Nucl. Phys. A 598 (1996) 390.
- [14] P. W. Anderson and P. Morel, Phys. Rev. 123 (1961) 1911.
- [15] Ø. Elgarøy, L. Engvik, E. Osnes, F. V. De Blasio, M. Hjorth-Jensen and G. Lazzari, Phys. Rev. Lett. 76 (1996) 1994.
- [16] M. Hoffberg, A. E. Glassgold, R. W. Richardson and M. Ruderman, Phys. Rev. Lett. 24 (1970) 775.
- [17] R. Tamagaki, Progr. Theor. Phys. 39 (1968) 91.
- [18] L. Amundsen, MSc. Thesis, University of Trondheim (1983), unpublished.
- [19] C. Schaab, F. Weber, M. K. Weigel and N. K. Glendenning, preprint astro-ph/9603142.
- [20] D. Page, Ap. J. 928 (1994) 250.
- [21] T. L. Ainsworth, J. Wambach and D. Pines, Phys. Lett. B 222 (1989) 173.
- [22] C. J. Pethick and D. G. Ravenhall, Texas/ESO-CERN Symposium on Relativistic Astrophysics, Cosmology, and Fundamental Physics Proceedings, J. D. Barrow, L. Mestel and P. A. Thomas (eds.), Ann. New York Acad. Sci. 647 (1991) 503